MNRAS 000, 1–5 (2015) Preprint 27 January 2016 Compiled using MNRAS LATEX style file v3.0

A ring-like concentration of mm-sized particles in Sz 91

H. Canovas,[1,2]⋆ C. Caceres,[1,2] M. R. Schreiber,[1,2] A. Hardy[1,2], L. Cieza[2,3], F. Ménard[4], A. Hales[5,6]

[1] *Departamento de Física y Astronomía, Universidad de Valparaíso, Valparaíso 2360102, Chile*
[2] *Millennium Nucleus "Protoplanetary discs in ALMA Early Science", Universidad de Valparaíso, Valparaíso 2360102, Chile*
[3] *Facultad de Ingeniería, Universidad Diego Portales, Av. Ejercito 441, Santiago, Chile*
[4] *UMI-FCA, CNRS/INSU, France (UMI 3386), and Departamento de Astronomía, Universidad de Chile, Casilla 36-D Santiago, Chile*
[5] *Atacama Large Millimeter/Submillimeter Array, Joint ALMA Observatory, Alonso de Córdova 3107, Vitacura 763-0355, Santiago - Chile*
[6] *National Radio Astronomy Observatory, 520 Edgemont Road, Charlottesville, VA, 22903-2475, USA*

arXiv:1601.06801v1 [astro-ph.SR] 25 Jan 2016

Accepted 2016 January 6. Received 2015 December 20; in original form 2015 November 16

ABSTRACT

Models of planet formation and disc evolution predict a variety of observables in the dust structure of protoplanetary discs. Here we present Atacama Large Millimeter/submillimeter Array (ALMA) Band-6 and Band-7 observations of the transition disc Sz 91 showing that the continuum emission at 870μm, which is dominated by emission from large dust grains, is localized in an optically thin narrow ring. We find that most of the emission ($\sim$ 95%) is concentrated in a ring located at 110 au from the central star that is only about 44 au wide. In contrast, the ^{12}CO (2-1) emission peaks closer to the star and is detected up to $\sim$ 488 au from the star. The concentration of large grains in a ring-like structure while the gas disc extends much further in and further out is in qualitative agreement with predictions of hydrodynamical models of planet-disc interactions including radial drift and gas drag.

Key words: protoplanetary discs – stars: variables: T Tauri – planet-disc interactions – stars: individual (Sz 91)

1 INTRODUCTION

The direct detection of giant planets in protoplanetary and debris discs (Lagrange et al. 2010; Quanz et al. 2013; Sallum et al. 2015) confirms that planets are born in protoplanetary discs. The detailed planet formation process, however, is rather poorly understood. For a long time, dust grains were expected to drift inwards on time-scales too fast to allow for significant growth of solids (Weidenschilling 1977). However, recent simulations suggest that radial-drift is not as effective as expected, showing that grains could survive the so called 'radial-drift barrier' (Laibe et al. 2012; Laibe 2014). High spatial resolution observations of potentially planet forming discs that allow the measurement of the radial distribution of dust grains are crucial to constrain the importance of radial drift for the planet formation process.

Models predict that a forming giant planet should carve a gap/cavity in its host protoplanetary disc, causing a pressure maximum at the inner edge of the disc. This has dramatic consequences on the distribution of dust particles. The larger particles in the outer disc drift inwards until they are held back near the pressure maximum (Paardekooper & Mellema 2006; Fouchet et al. 2007). On the other hand, small particles ($\lesssim 10\mu$m) do not accumulate at the pressure maximum and are allowed to enter the cavity (e.g. Rice et al. 2006). Thus, if a giant planet has carved a gap or cavity inside a protoplanetary disc, an accumulation of large particles in a ring-like structure close to the inner edge of the outer disc is expected (Pinilla et al. 2012). The sizes of the particles affected by this filtering/trapping mechanism depend on the exact shape of the pressure bump which mostly depends on the planet mass (Gonzalez et al. 2012; de Juan Ovelar et al. 2013). The two key ingredients of this scenario, dust filtration and radial drift, are supported by recent observations. The different cavity sizes found for different grain sizes in several transition discs confirm dust filtration (e.g., Garufi et al. 2013). Furthermore, radial drift triggered by gas drag (Birnstiel & Andrews 2014) can explain the observed difference in the outer radii of the gas and dust components of protoplanetary discs (e.g., Panić et al. 2009; Andrews et al. 2012; de Gregorio-Monsalvo et al. 2013).

In this work we present ALMA cycle 2 data of the transition disc Sz 91. This young system (age $\sim$ 1Myr, $M_\star$ 0.47 $M_\odot$, $T_\star$ 3720 K, see Canovas et al. 2015, hereafter C2015, for details) is located in the Lupus III star forming region at a distance of 200 pc (Merín et al. 2008), and

⋆ E-mail: hector.canovas@dfa.uv.cl

© 2015 The Authors

was first classified as a potentially planet forming disc by Romero et al. (2012) based on its SED. Further observations revealed that Sz 91 has remarkably different cavity sizes as a function of wavelength: ~ 65 au in radius at K_s band (Tsukagoshi et al. 2014), which is sensitive to small grains, and ~ 97 au at 1.3 mm (C2015), which traces large grains. The outer edge of the gaseous disc has also been detected further than the continuum emission at 1.3 mm (C2015). However, due to the resolution and sensitivity of these observations, it was previously not possible to assess whether that discrepancy was due to a physical difference between the radial distribution of gas and large dust, or due to an observational effect. The accretion rate (7.9×10^{-11}Myr^{-1}) and huge cavity exclude photoevaporation as the mechanism responsible for the gap formation and the lack of a detected stellar companion makes Sz 91 one of the strongest candidates for a planet forming disc (C2015). Our new observations further support this hypothesis. The new data shows that large grains are distributed in a narrow, ring-like structure as predicted by models of planet-disc interactions, while ^{12}CO (2-1) is detected much further out from the central star. This accumulation of dust may facilitate the growth of solids.

2 OBSERVATIONS

Sz 91 was observed with ALMA in band-6 and band-7 with two different configurations during Cycle-2 (programme 2013.1.00663.S, PI: Canovas).

In Band 6, 40 (12-m) antennas were used during the observations with baselines ranging from 23.3 to 558.2 m (17.9 to 429.4 kλ). The ALMA correlator was configured to provide one continuum spectral window with a total bandwidth of 2 GHz centred at 231.6 GHz and three spectral windows with bandwidths of 58.6 MHz and channel widths of 61.035 KHz. These narrow windows were centred on the ^{12}CO (2-1, 230.5 GHz) (hereafter ^{12}CO), ^{13}CO (2-1, 220.4 GHz), and C^{18}O (2-1, 230.5 GHz) lines.

The Band 7 observations were performed with 42 (12-m) antennas with baselines ranging from 15.1 to 1574.4 m (17.3 to 1789.1 kλ). The correlator was configured to provide two continuum spectral windows with a total bandwidth of 2 GHz centred at 332.5 and 343.7 GHz, and two spectral windows with bandwidths of 58.6 MHz and channel widths of 61.035 KHz aimed to measure the ^{12}CO (3-2, 345.8 GHz) and ^{13}CO (3-2, 330.6 GHz).

The quasars QSO J1517-2422 and QSO J1610-3958 were observed for bandpass and phase calibration. Titan and Ceres were observed to perform flux calibration in Band 6 and Band 7, respectively. The uncertainty associated with the flux calibration is ~ 10% (ALMA Cycle 3 Technical Handbook). Water vapor was continuously monitored with the radiometers attached to each antenna to correct for the fast fluctuations of the phase. In both bands the individual exposure times were 6.05 s, amounting to a total exposure time for the science observations of 207 and 1430 s in Band 6 and Band 7, respectively. The median precipitable water vapor (PWV) was 0.67 mm and 1.15 for Band 6 and Band 7, respectively.

In this letter we focus on the observational constraints derived from the Band 7 continuum and the ^{12}CO moment maps, as they provide the best trade-off between spatial resolution and sensitivity. A detailed model of the dusty and gaseous disc is beyond the scope of this letter and will be presented in a forthcoming paper.

We used CASA (McMullin et al. 2007) to process the visibilities. Channels showing artefacts were flagged out. The line-free channels were used to fit and subtract the continuum to the emission-line bearing channels. The CLEAN algorithm (Högbom 1974) was applied to deconvolve the visibilities using Briggs and natural weighting for the ^{12}CO and continuum, respectively. We applied one round of self-calibration finding a marginal increment in S/N, so no more iterations were applied. The median rms in the continuum is 0.95 mJy beam^{-1} with a beam size of 0.21 arcsec × 0.15 arcsec (42 × 30 au) and position angle (PA) of 79.9°. The beam size in the ^{12}CO data is 0.60 arcsec × 0.57 arcsec (120 × 114 au) and PA of 84.2°. The ^{12}CO is detected above 3σ at velocities ranging from 0.320 to 5.040 km s^{-1} (LSRK), with a median rms in the line-free channels of 20.12 mJy beam^{-1}.

3 RESULTS

3.1 Continuum

The continuum image (Fig. 1, left) shows an inclined narrow ring with a large central hole clearly resolved. The peak flux is 2.17 ± 0.95 mJy beam^{-1}. Integrating the flux inside the regions with S/N > 3σ results in $F_{1.3mm}$ 40.15 ± 0.95 mJy. We derive the geometry of the continuum disc by fitting a ring profile to the continuum visibilities using *uvfit*/MIRIAD. We find that the disc's centre is offset by $\Delta\alpha$ 0.10 arcsec ± 0.004 arcsec and $\Delta\delta$ -0.02 arcsec ± 0.004 arcsec from the ALMA phase centre (α_{2000} $16^h07^m11^s.56$ and δ_{2000} $-39°03'47''.82$). We derive a PA = 17.4±0.4°, inclination i 51.7 ± 0.4°, and a total flux of 42.43 ± 0.95 mJy. This value is slightly higher than previously reported observations at the same wavelength (Romero et al. 2012; Tsukagoshi et al. 2014), and we consider it very likely that this difference is a consequence of calibration uncertainties.

The hole of the ring shows no emission above the rms of our images. The emission at the ring's ansae is higher than in the rest of the ring. This can be naturally explained by a combination of the disc's inclination and optically thin emission, as there is more dust emitting along the line of sight of the major axis.

The dust mass of the ring can be roughly estimated using the linear relations derived by Andrews & Williams (2005, 2007) and calibrated by Cieza et al. (2008):

$$M_{\rm dust} \sim 8.0\times10^{-5}\,[\frac{F_\nu 0.86\ {\rm mm}}{\rm mJy}\times\frac{d}{140\ {\rm pc}}^2]\ M_{\rm Jup}, \qquad (1)$$

where d is the distance to the disc. Using a distance of 200 pc (Merín et al. 2008), the measured total flux, and 10% uncertainties for the flux and distance, we derive a total mass of 23 ± 6 $M_{\rm Earth}$, in agreement with previous estimates for the disc's mass in large grains (Romero et al. 2012; Tsukagoshi et al. 2014; Canovas et al. 2015). However we are cautious about this result as a major assumption in this method is that the grain size distribution follows an interstellar medium (ISM) distribution with power law index p −3.5 (Mathis et al. 1977), and this may not be the case when the dust population is dominated by large grains. A detail model

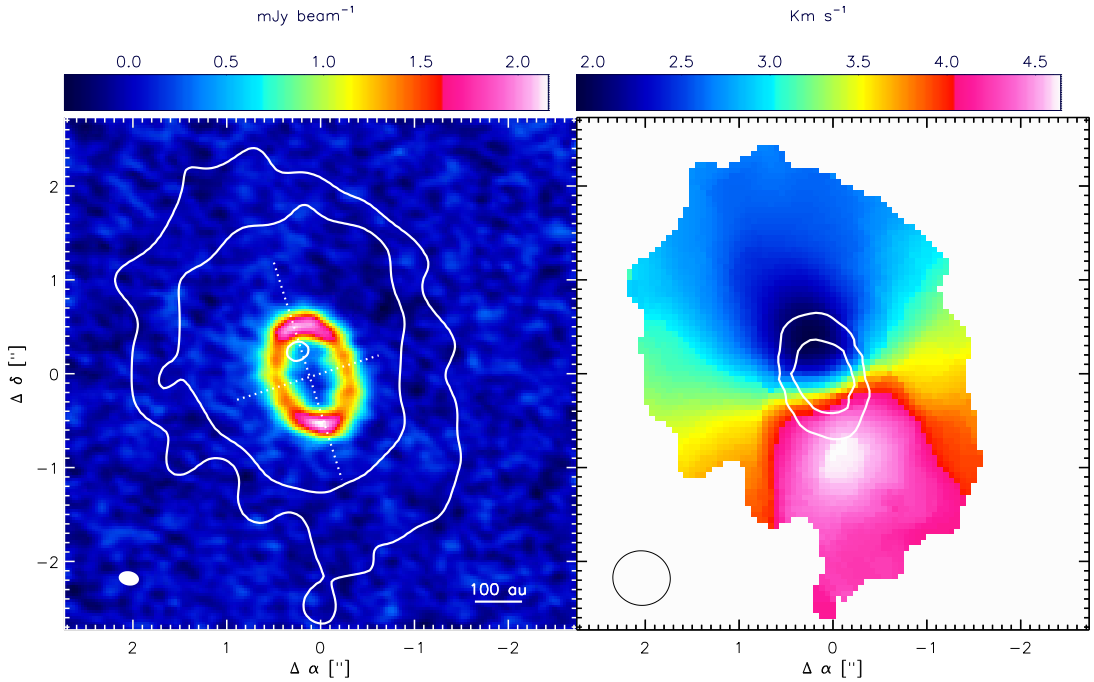

Figure 1. Left: cleaned continuum image at band-7 (870μm). The dotted cross shows the disc's centre and major/minor axis derived in Sect. 3.1. White lines contour the ^{12}CO integrated intensity (Moment-0) map at 2.5, 15, 31× rms (22.7mJy beam^{-1}km s^{-1}), highlighting that the ^{12}CO emission is detected much further out than the continuum emission. The ^{12}CO emission peaks inside the ring's hole, at ~ 60 au. The asymmetric profile is a consequence of the cloud contamination (see text). **Right:** ^{12}CO velocity field (Moment-1) map. The white lines contour the 10× rms (0.1 mJy) of the continuum emission. The synthesized beam of the continuum and ^{12}CO observations is shown in the bottom-left corner of the left and right figures, respectively.

exploring different possible scenarios is needed to better constrain the mass in the ring but this is beyond the scope of this letter.

3.2 ^{12}CO Moments

In order to evaluate the total extension of the gaseous disc, we created the Moment-0 (velocity-integrated intensities) and Moment-1 (intensity-weighted velocities) images from the channels showing significant ($> 3\sigma$) emission. Pixels with values below 2.5× the median rms (20.12 mJy beam^{-1}) were excluded from these computations. A Gaussian profile was fitted along the spectral axis at each spatial position to ensure that the full ^{12}CO profile was included at each location. The Moment-0 has an rms of 22.7 mJy beam^{-1}km s^{-1} and its integrated flux is 4.932 ± 0.023 Jy km s^{-1}. Fig. 1 (right) displays the Moment-1 in colours encompassing the 2.5×rms region of the Moment-0. The asymmetric shape of the images is a consequence of the filtering-out of the interferometer due to cloud emission at $v_{\rm LSRK} > 3.8$ km s^{-1}, which translates to a reduced flux in the red-shifted side of the ^{12}CO line (previously noticed by Tsukagoshi et al. 2014; Canovas et al. 2015). The blue-shifted side, unaffected by the cloud, shows ^{12}CO emission up to ~ 2.44 arcsec (~488 au) from the disc's centre, and peaks at 60 ± 12 au, inside the hole of the ring and near the cavity edge observed at $K_{\rm s}$ band (Tsukagoshi et al. 2014).

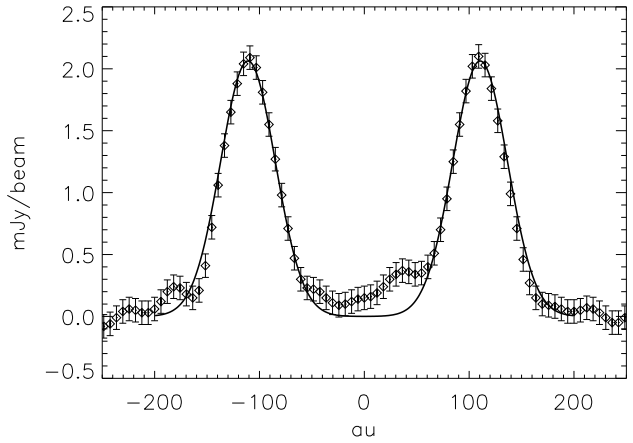

Figure 2. Cut along major axis of the Band-7 continuum disc. Error bars represent the rms of the observations; the peak is detected with a signal to noise of S/N~22. Positive distance points to the north direction, and negative distance to the south direction. The ring has same width and peak values along the northern and southern sides. Inside the hole, there is a small excess ($\lesssim 3\sigma$) of emission along the northern side when compared to its southern counterpart. The solid curve represents the best fit described in Sect. 3.3.

3.3 Surface brightness profile of mm emission

To derive further constraints on the ring geometry we use the brightness profile along the major axis of the ring. We find that the emission is concentrated in a narrow ring be-

tween ~ 60 and ~ 150 au from the central star, with the peak emission at ~ 110 au (Fig. 2). Averaging the emission in ellipsoids which have the same inclination and PA as the disc provides the same results. We then fit three different brightness profiles to the surface brightness profile along the major axis: a Gaussian, a constant (hat-like), and a power-law with exponent −1.0. We vary the widths and central positions of these profiles, and convolve them with a Gaussian function of full width at half-maximum FWHM = 0.16 arcsec (i.e., equal to the FWHM of the continuum synthesized beam along the disc's major axis) to compare with the observations. We then perform a Monte Carlo Markov Chain (MCMC) exploration to identify the best fit to the observations. We find that a Gaussian profile centred at 110.5 ± 0.3 au and with 1σ width of 22.2 ± 0.5 au results in the best fit to our observations, with reduced χ^2_ν 1.27 (Fig. 2). For comparison, the hat-like and the power-law distribution result in χ^2_ν 1.61 and χ^2_ν 2.39, respectively. Our best fit implies that 95.5% of the dust probed by our Band-7 observations is located within 88 – 132 au.

4 DISCUSSION

The ALMA Cycle-2 observations presented here have much higher sensitivity and spatial resolution than previous observations. They reveal two striking features: (1) there is a large difference between the outer disc radius of the large grains and the ^{12}CO disc, and (2) the large grains are concentrated in a narrow, ring-like structure. The difference in the outer edges of the gaseous and continuum discs cannot be explained by beam dilution or sensitivity effects, and overall our observations show that the radial distribution of the large particles probed by the continuum images is very different from the radial distribution of the gas.

4.1 Sz 91 radial structure

The spectral energy distribution (SED) of Sz 91 indicates that the innermost regions of the disc must contain a very small amount of dust to simultaneously reproduce the excess emission at 12μm and the absence of emission above photospheric levels at wavelengths below 10μm (Romero et al. 2012; Tsukagoshi et al. 2014; Canovas et al. 2015). Imaging polarimetry observations with SUBARU at K_s band resolved the disc showing that Sz 91 has a ~ 65 au cavity in its μm-sized grain distribution (Tsukagoshi et al. 2014) while ALMA Band-6 (1.3 mm) Cycle-0 observations revealed that the radius of the cavity is significantly larger for mm-sized particles, i.e. ~ 97 au (C2015). Combining these observational constraints and the observations presented in this work, and taking into account that the small grains are well coupled to the gas (Fouchet et al. 2007), a complex radial structure emerges. The distribution of small grains is severely depleted inside the inner ~ 65 au, and extends beyond 400 au. On the other hand, the large grains that contain the bulk of the disc mass in dust are concentrated in a ring. Most of the emission is located between ~ 88 and ~ 132 au. As shown by C2015, ^{12}CO is detected down to ~ 28 au from the star, well inside the ring's hole.

4.2 A planet-induced pile up?

Several observations of transition (e.g., Andrews et al. 2012; Rosenfeld et al. 2013; Walsh et al. 2014) and protoplanetary discs (e.g. Panić et al. 2009; de Gregorio-Monsalvo et al. 2013) show that the gaseous disc extends further out than the dusty disc. In all these cases, radial drift of large particles (Birnstiel & Andrews 2014) has been invoked as the natural explanation for these discrepancies. In the case of Sz 91, the differences in the outer edges of the ^{12}CO disc and the geometry of the distribution of large particles (inner and outer edges), indicates that there must be at least one other mechanism in action. The effect of multiple giant planets orbiting inside the cavity seems plausible, given the observed characteristics of this object (see C2015 for a detailed discussion). The different cavity sizes for the small and large grain distributions are in agreement with the predictions of recent hydrodynamical simulations of multiple planets embedded in a disc (Dong et al. 2015; Pinilla et al. 2015). Hydrodynamical models describing the planet-disc interactions including radial drift predict that the large grains will concentrate at the pressure maximum created by an orbiting planet, resulting in a narrow, ring-like structure (Gonzalez et al. 2012; Pinilla et al. 2012). Our observations are in agreement with these predictions.

While it is clear that the mm sized particles are located in a narrow ring, our observations are unable to tell if the observed structure represents a stationary state. If the torque created by the orbiting planets equals the drift torque this would be the case but it might also be that the large grains are currently still in the process of piling up.

5 CONCLUSIONS

In this letter we present ALMA Cycle 2 observations of the continuum at 870μm and ^{12}CO of the transition disc Sz 91. The images reveal that the distribution of the gas and the large grains is very different, with the large particles detected up to ~ 150 au while the gas is detected up to ~ 488 au. We find that a Gaussian profile centred at 110.5 ± 0.3 au and with 1σ width of 22.2 ± 0.5 au provides the best fit to our observations, which means that most of the continuum emission is located in a narrow ring between ~ 88 – 132 au. Our findings are in qualitative agreement with predictions of a pile-up of large grains due to a combination of pressure bumps created by low-mass companions, and radial drift triggered by gas drag (Pinilla et al. 2012; de Juan Ovelar et al. 2013). This concentration of large grains could facilitate the formation process of further planets as the particles may grow faster because of enhanced density of solids.

The hole at (sub)mm wavelengths is surprisingly large when compared with transition discs around low-mass stars (e.g., Andrews et al. 2011) which, together with its moderate accretion rate, suggests the presence of multiple planets inside the hole (Dodson-Robinson & Salyk 2011). The presence of a small amount of μm-sized grains in the innermost regions of the disc, the difference in cavity radii between the μm grains and mm-sized grains, and the pile-up of large grains in a narrow ring, are consistent with a giant planet orbiting at the inner edge of the ~ 65 au cavity observed at K_s band (de Juan Ovelar et al. 2013). Given the wealth

of signposts of planet-disc interactions in Sz 91, we consider this object an ideal laboratory with which to test model predictions for planet formation, planet disc interaction, and protoplanetary disc evolution around low-mass stars.

ACKNOWLEDGEMENTS

We thank the referee for his/her useful comments and suggestions. HC acknowledges support from ALMA/CONICYT (grants 31100025 and 31130027). CC and MRS acknowledge support from FONDECYT grants 3140592 and 1141269. AH is supported by Doctoral scholarship FIB-UV 2014 and Gemini/Conicyt 32120033 LC and FM acknowledge funding from CONICYT FONDECYT #1140109 and the EU FP7-2011 (Grant Agreement no. 284405), respectively. This paper makes use of the following ALMA data: ADS/JAO.ALMA#2011.0.00733.S. ALMA is a partnership of ESO (representing its member states), NSF (USA) and NINS (Japan), together with NRC (Canada), NSC and ASIAA (Taiwan), and KASI (Republic of Korea), in cooperation with the Republic of Chile. The Joint ALMA Observatory is operated by ESO, AUI/NRAO and NAOJ. The National Radio Astronomy Observatory is a facility of the National Science Foundation operated under cooperative agreement by Associated Universities, Inc.

REFERENCES

Andrews S. M., Williams J. P., 2005, ApJ, 631, 1134
Andrews S. M., Williams J. P., 2007, ApJ, 671, 1800
Andrews S. M., Wilner D. J., Espaillat C., Hughes A. M., Dullemond C. P., McClure M. K., Qi C., Brown J. M., 2011, ApJ, 732, 42
Andrews S. M., et al., 2012, ApJ, 744, 162
Birnstiel T., Andrews S. M., 2014, ApJ, 780, 153
Canovas H., et al., 2015, ApJ, 805, 21
Cieza L. A., Swift J. J., Mathews G. S., Williams J. P., 2008, ApJ, 686, L115
Dodson-Robinson S. E., Salyk C., 2011, ApJ, 738, 131
Dong R., Zhu Z., Whitney B., 2015, ApJ, 809, 93
Fouchet L., Maddison S. T., Gonzalez J.-F., Murray J. R., 2007, A&A, 474, 1037
Garufi A., et al., 2013, A&A, 560, A105
Gonzalez J.-F., Pinte C., Maddison S. T., Ménard F., Fouchet L., 2012, A&A, 547, A58
Högbom J. A., 1974, A&AS, 15, 417
Lagrange A.-M., et al., 2010, Science, 329, 57
Laibe G., 2014, MNRAS, 437, 3037
Laibe G., Gonzalez J.-F., Maddison S. T., 2012, A&A, 537, A61
Mathis J. S., Rumpl W., Nordsieck K. H., 1977, ApJ, 217, 425
McMullin J. P., Waters B., Schiebel D., Young W., Golap K., 2007, in Shaw R. A., Hill F., Bell D. J., eds, ASP Conf. Ser. Vol. 376, Astronomical Data Analysis Software and Systems XVI. p. 127
Merín B., et al., 2008, ApJS, 177, 551
Paardekooper S.-J., Mellema G., 2006, A&A, 453, 1129
Panić O., Hogerheijde M. R., Wilner D., Qi C., 2009, A&A, 501, 269
Pinilla P., Benisty M., Birnstiel T., 2012, A&A, 545, A81
Pinilla P., de Juan Ovelar M., Ataiee S., Benisty M., Birnstiel T., van Dishoeck E. F., Min M., 2015, A&A, 573, A9
Quanz S. P., Amara A., Meyer M. R., Kenworthy M. A., Kasper M., Girard J. H., 2013, ApJ, 766, L1
Rice W. K. M., Armitage P. J., Wood K., Lodato G., 2006, MNRAS, 373, 1619
Romero G. A., Schreiber M. R., Cieza L. A., Rebassa-Mansergas A., Merín B., Smith Castelli A. V., Allen L. E., Morrell N., 2012, ApJ, 749, 79
Rosenfeld K. A., Andrews S. M., Wilner D. J., Kastner J. H., McClure M. K., 2013, ApJ, 775, 136
Sallum S., et al., 2015, Nature, 527, 342
Tsukagoshi T., et al., 2014, ApJ, 783, 90
Walsh C., et al., 2014, ApJ, 791, L6
Weidenschilling S. J., 1977, MNRAS, 180, 57
de Gregorio-Monsalvo I., et al., 2013, A&A, 557, A133
de Juan Ovelar M., Min M., Dominik C., Thalmann C., Pinilla P., Benisty M., Birnstiel T., 2013, A&A, 560, A111

This paper has been typeset from a TEX/LATEX file prepared by the author.